REPORT DOCUMENTATION PAGE

AFRL-SR-BL-TR-98-

0647

1. AGENCY USE ONLY (Leave blank)	2. REPORT DATE	3. REPORT
	31 August 1998	Final 4-1-95 to 3-31-98

4. TITLE AND SUBTITLE

New Approaches to Aluminum Passivation for Corrosion Prevention

5. FUNDING NUMBERS

2303/BS
61102F

6. AUTHOR(S)

John T. Yates, Jr.

7. PERFORMING ORGANIZATION NAME(S) AND ADDRESS(ES)

University of Pittsburgh
Department of Chemistry
Surface Science Center
Pittsburgh, PA 15260

8. PERFORMING ORGANIZATION REPORT NUMBER

9. SPONSORING/MONITORING AGENCY NAME(S) AND ADDRESS(ES)

AFOSR/NL
Building 410
Bolling AFB, DC 20332-6448

Mai Delong

10. SPONSORING/MONITORING AGENCY REPORT NUMBER

F49620-95-1-0186

11. SUPPLEMENTARY NOTES

12a. DISTRIBUTION/AVAILABILITY STATEMENT

Approved for public release: Distribution is unlimited

12b. DISTRIBUTION CODE

13. ABSTRACT (Maximum 200 words)

A new method for producing an aluminum oxide film on an aluminum surface has been discovered. This method involves the activation of adsorbed H_2O molecules by the attachment of low energy electrons-producing OH radicals which are aggressive oxidizing agents. Al_2O_3 film thicknesses of up to 25 Å are easily achieved. Al_2O_3 films made this way are excellent for corrosion passivation as measured electrochemically, and the artificially produced films exhibit a factor of 15-20 x higher impedance than thermally-grown Al_2O_3 films of the same thickness. In addition the stability of two aluminum corrosion inhibitor molecules on Al_2O_3 has been separately investigated using FTIR spectroscopy.

14. SUBJECT TERMS

aluminum
corrosion passivation
aluminum oxide
dissociative electron attachment
benzotriazole
vinyltriethyoxy silane

15. NUMBER OF PAGES 28

16. PRICE CODE

17. SECURITY CLASSIFICATION OF REPORT	18. SECURITY CLASSIFICATION OF THIS PAGE	19. SECURITY CLASSIFICATION OF ABSTRACT	20. LIMITATION OF ABSTRACT
Unclassified	Unclassified	Unclassified	

FINAL REPORT

New Approaches to Aluminum Passivation for Corrosion Prevention

Grant No: F49620-95-1-0186

31 August 1998

John T. Yates, Jr.
University of Pittsburgh
Department of Chemistry
Surface Science Center
Pittsburgh, PA 15260

I. Objective

The objective of this research was to discover new methods for producing a corrosion passivation layer on aluminum surfaces, and for measuring the degree of corrosion passivation using electrochemical methods. This objective has been achieved. The work was divided into two parts. In the first part, an Al(111) single crystal surface was employed to study the activation of adsorbed water molecules with low energy electrons, leading to an artificial oxide layer. In the second part, the method developed in the work with the Al(111) crystal was applied to many polycrystalline Al samples and the artificial oxide films produced were then tested by electrochemical impedance spectroscopy for their ability to retard electrochemical corrosion. In the third part of the work, two corrosion inhibitor molecules were studied as adsorbates on an Al_2O_3 surface, and their thermal behavior was monitored by FTIR spectroscopy.

II. Status of Effort - Producing a Better Barrier Oxide Layer

A. Electronic vs. Thermal Activation of Surface Reactions

Figure 1 shows a schematic diagram in which a thermally activated surface chemical reaction is shown in the top panel. Here, thermal energy supplied to the reactants causes the system to progress from the reactant to the product over a single potential energy surface containing an activation energy barrier. This is the conventional route for activating a surface chemical reaction by heating, and the system is at thermal equilibrium as reactant molecules are converted to product molecules.

In contrast, electronically-activated surface reactions, stimulated by

electrons or by photons, produce reactant molecules on an excited state potential energy surface such as in the example shown in the bottom panel of Figure 1, where electron attachment to the reactant molecule X produces the temporary negative ion state, X^-. The X^- species either converts to a product which involves bond breaking in X^-, or it is quenched back to an excited vibrational state of the original undissociated X molecule. This vibrationally excited molecule may then convert to the dissociated products because of the excess vibrational energy which it contains. In either case, the system has been pushed far from thermal equilibrium as a result of excitation in the initial electron attachment process, and enhanced chemical activity is observed.

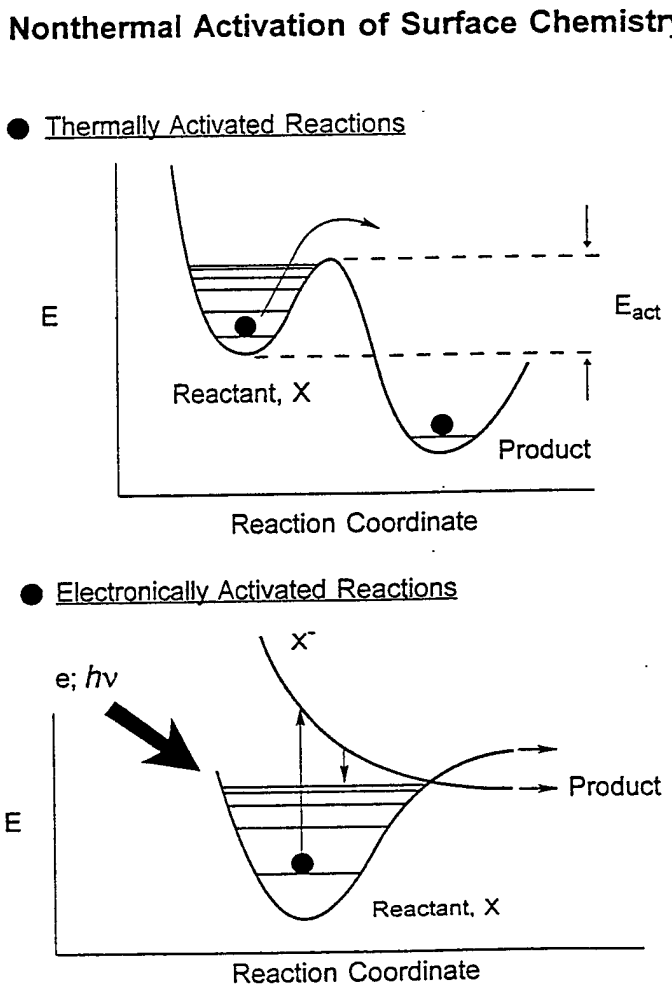

Figure 1. Comparison of thermal and nonthermal activation of surface chemistry.

B. Electron Beam Activation of H_2O on Al(111) at 90 K to Produce Al_2O_3

Experiments were first conducted with H_2O layers condensed on an atomically clean Al(111) surface. At 90 K, water does not react with Al(111) so that any reaction observed can be attributed to excitation by the incident electrons rather than to thermal excitation processes. As shown in Figure 2, in an exploratory experiment, a 3 keV electron beam produces a deposit of a non-volatile oxide in the region irradiated by the beam. The oxygen-containing product, later shown to be Al_2O_3, was locally deposited, as indicated by the Auger spectrum obtained after heating to 673 K to vaporize unreacted H_2O. The width of the Al_2O_3 profile is larger than the electron beam profile, and this is probably due to the influence of secondary electrons produced by the incident 3 keV electrons. The secondary electrons are emitted in a wide solid angle in the backward direction, exiting the surface and producing additional Al_2O_3 by excitation of H_2O molecules adsorbed at the perimeter of the incident electron beam.

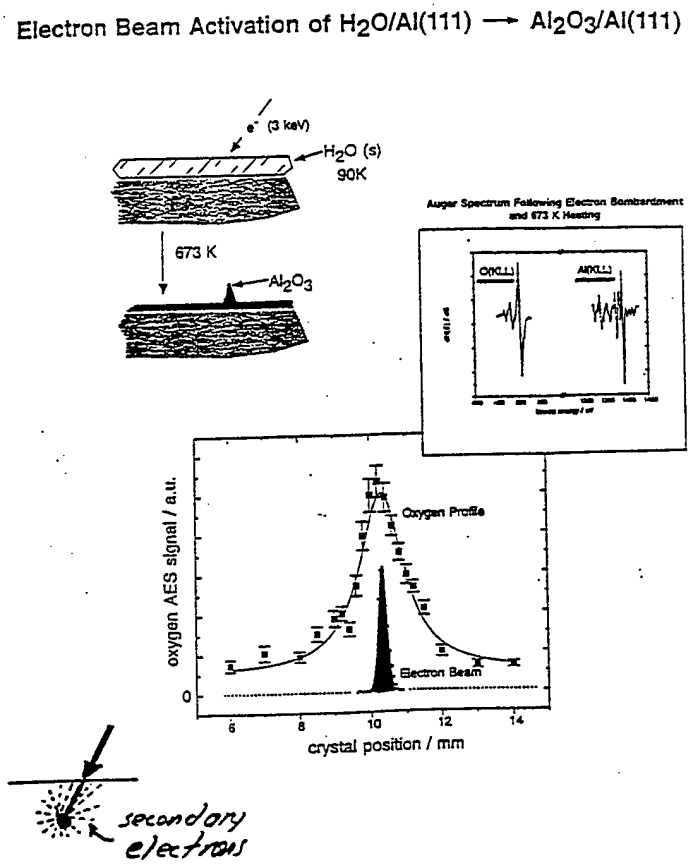

Figure 2. Electron beam activation of H_2O/Al(111) at 90 K.

Using a wide beam electron gun designed specially for this work, the H_2O/Al(111) surface at 90 K was uniformly irradiated over its entire front surface with 100 eV electrons, and the conversion of H_2O to Al_2O_3 was followed using XPS, as shown in Figure 3. A 2.4 eV downshift in the O(1s) binding energy occurs as water is destroyed and as Al_2O_3 is produced [1].

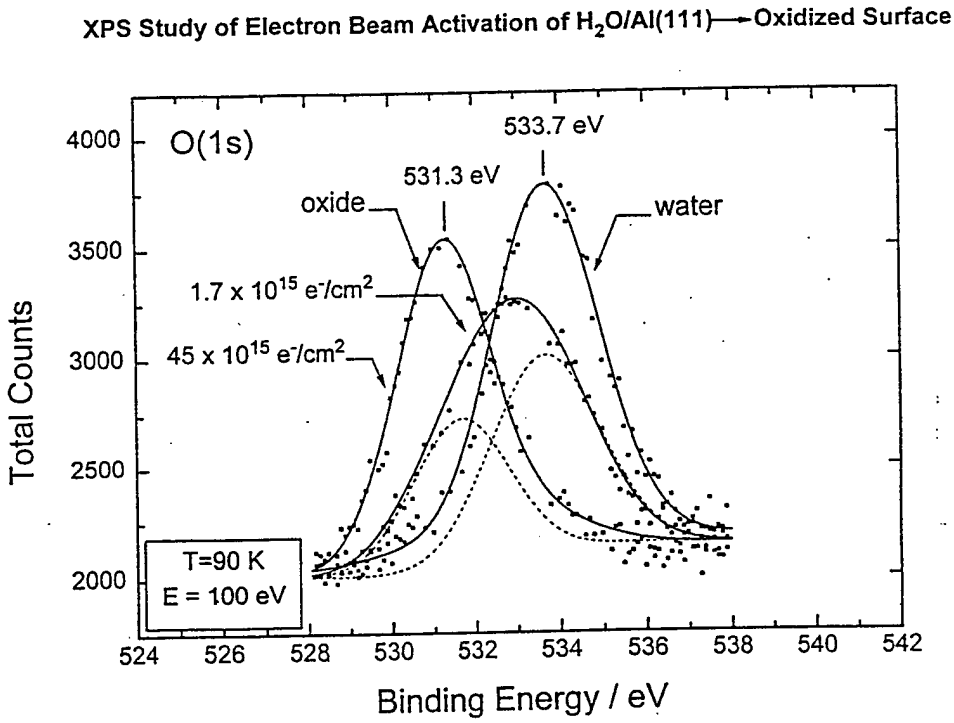

Figure 3. XPS study of the activation of H_2O/Al(111) by a broad uniform electron beam at a surface temperature of 90 K [1].

The efficiency of the conversion process was measured, using the integrated O(1s) intensity decay of the H_2O and the integrated O(1s) intensity gain of the Al_2O_3. These results are shown in Figure 4, and two important conclusions may be reached.

1. The cross section for conversion of a H_2O molecule in a thick ice layer to aluminum oxide is about 2×10^{-16} cm^2 for 100 eV electrons. This corresponds to a **very high efficiency** of the surface reaction in which each incident electron exhibits almost unit efficiency in causing the oxidation reaction.

2. The conversion of H_2O to Al_2O_3 is quantitative, since the total oxygen coverage, as measured by the total integrated O(1s) signal, remains almost constant.

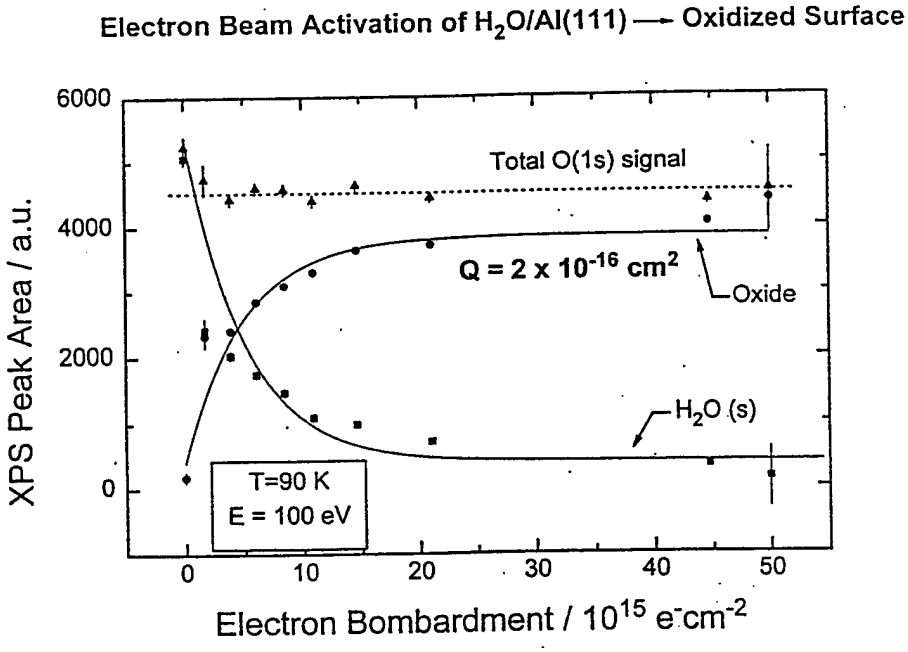

Figure 4. Electron beam conversion of H_2O/Al(111) to Al_2O_3/Al(111) at 90 K as measured by XPS[1].

The nature of the excitation responsible for this process was investigated by measuring the rate of Al_2O_3 production as a function of the incident electron energy. It was found that the threshold electron energy for the excitation was at 8 eV laboratory energy, uncorrected for work function differences, as shown in Figure 5. After a correction for the measured work function difference between the electron emitter and the surface, the threshold electron energy for the excitation of water to produce the oxide is 6 ± 1 eV.

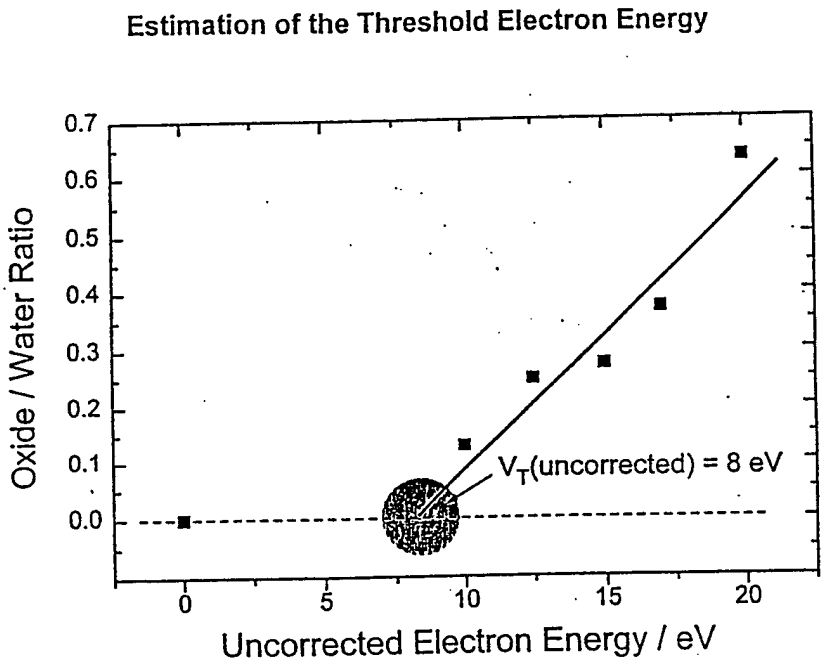

Figure 5. Estimation of the threshold electron energy for the oxidation of Al(111) by electron bombardment of H_2O/Al(111) at 90 K [1].

Studies of the electronic excitation of gas phase H_2O molecules reveal that there are three distinct resonance energies at 6.4, 8.4, and 11.2 eV, where an electron may be captured to form an excited temporary $(H_2O^*)^-$ negative ion. The measured 6 eV threshold electron energy for the oxidation process on Al(111) is consistent with the excitation of the lowest H_2O resonance energy. Most likely, the reaction occurs with the production of a hydrogen anion and a chemically reactive OH radical [2-4], as shown schematically in Figure 6. The OH radical is then responsible for the facile oxidation of the Al(111) surface. Recently, the oxidation of a hydrogen-terminated silicon surface by adsorption of water followed by electron bombardment has been determined to be partly due to this process [5].

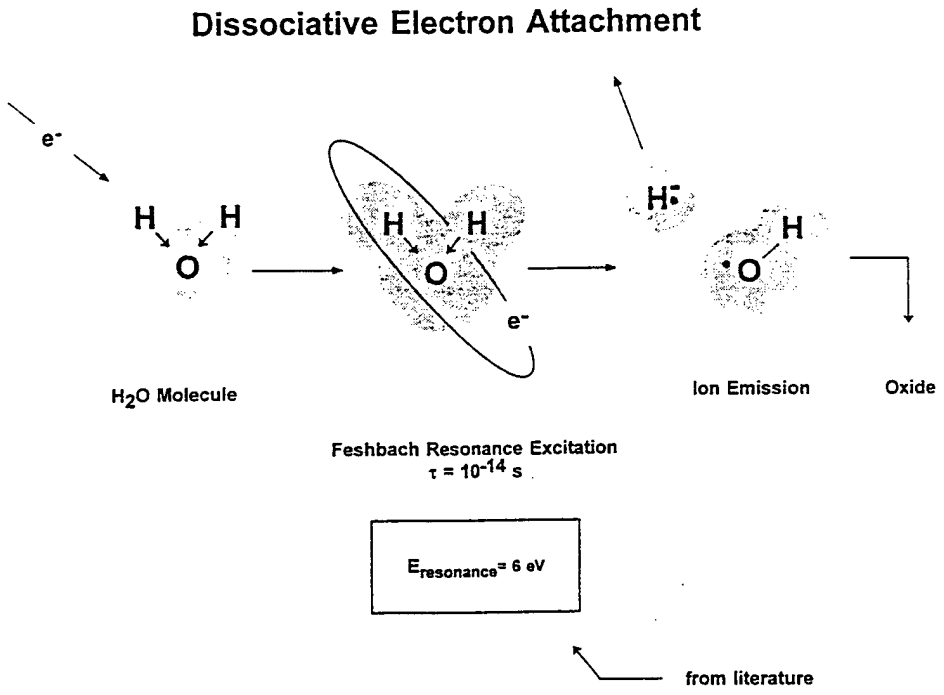

Figure 6. Dissociative electron attachment-Schematic view of the production of a temporary negative ion which leads to the dissociation of the molecule, producing chemically active fragments.

C. Electron Beam Activation of H_2O/Al(111) at 300 K to Produce Al_2O_3

The studies shown above were carried out at 90 K in order to eliminate any possibility of interference from thermal oxidation reactions. A more practical temperature for the use of electron beam activation of adsorbed water to produce Al_2O_3 films is 300 K, and extensive studies were therefore performed at this temperature [6]. A background flux of water vapor (5×10^{-7} Torr) was combined with a 100 eV electron beam flux of $10\mu A/cm^2$. Under these low gas density conditions, no gas phase excitation events would be expected, and the reaction initiated by electrons therefore involves only the excitation of adsorbed species. Under these conditions, the activation of adsorbed H_2O molecules is efficiently achieved as indicated in Figure 7.

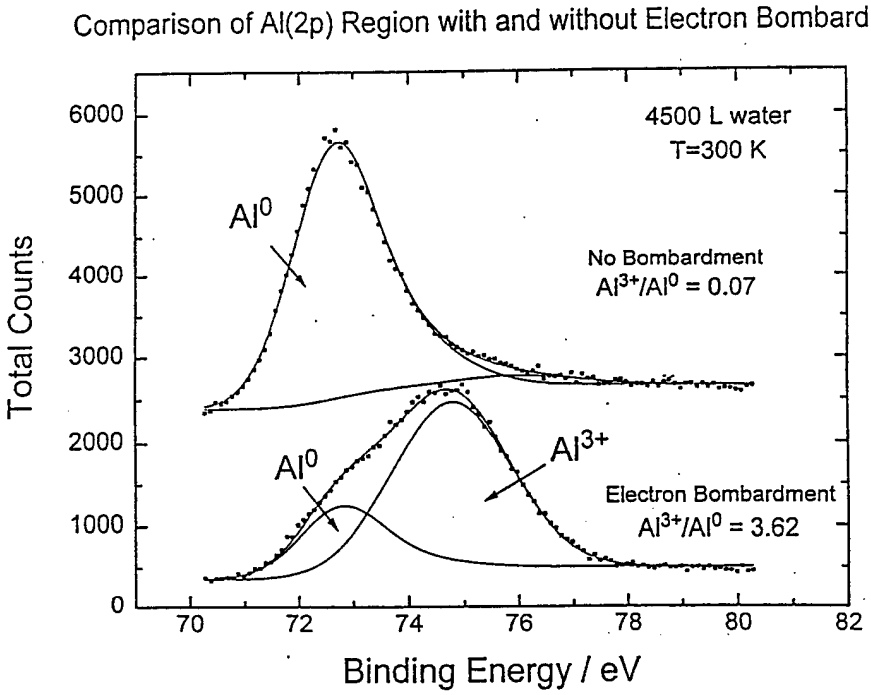

Figure 7. XPS comparison of Al(2p) region with and without electron bombardment [6].

The production of Al^{+3} by the electron stimulated process is evident from Figure 9. This process has been shown to produce a thick oxide film with a **linear growth kinetic law** up to a shutdown point which occurs at a film thickness of about 25 Å. In contrast, the normal Mott-Cabrera mechanism for thermally-activated oxide film growth exhibits a **parabolic growth kinetic law** in which the film thickness increased as $t^{½}$ Figure 8 indicates the linear kinetic growth of the oxide film during sequential 900 s steps of electron bombardment under constant H_2O flux and electron flux conditions. The much slower growth of an oxygen-containing layer from exposure to H_2O without electron bombardment is shown also in Figure 8.

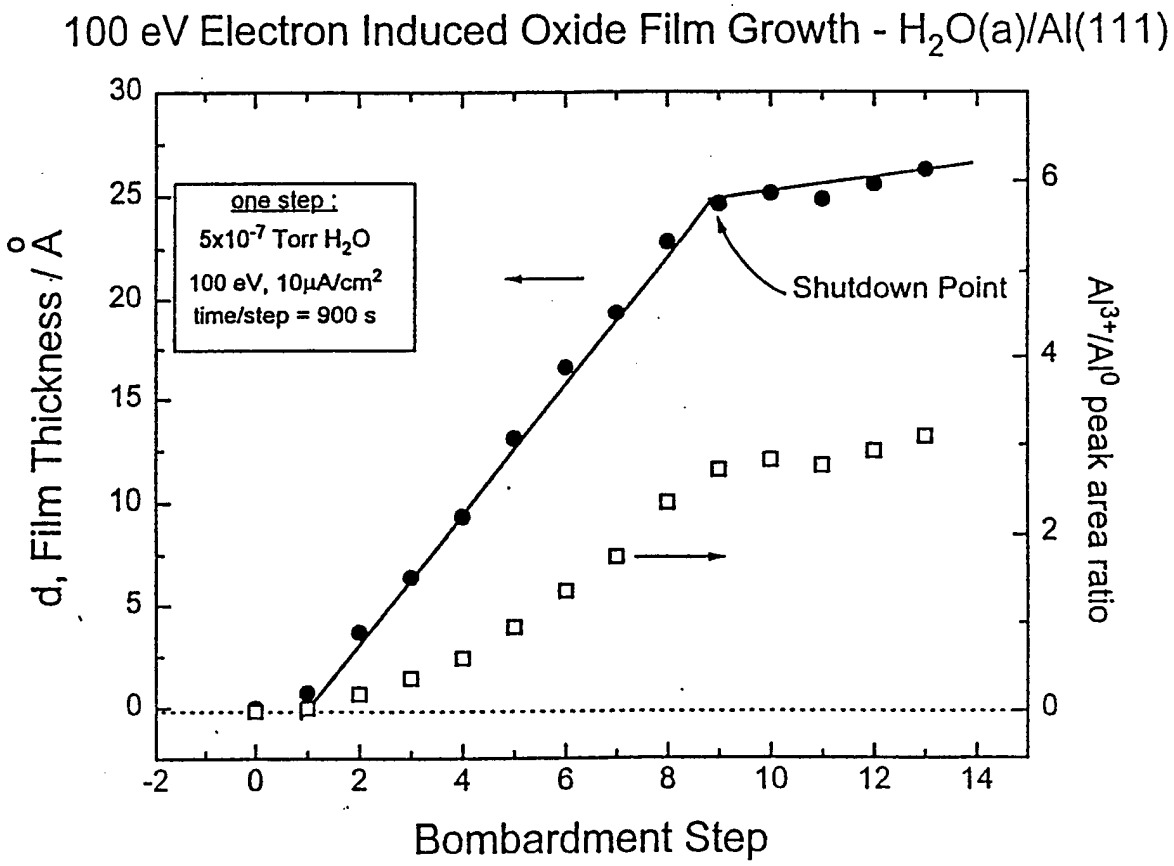

Figure 8. Electron induced oxide film growth- H_2O/Al(111), 300 K [6].

During the film growth, the XPS analytical procedure is able to measure the stoichiometric ratio of Al^{+3} to O for the growing layer. At low film thicknesses, this Al^{+3}/O ratio will be low because of the measurement of the combined O(1s) signal from water, from surface hydroxyl groups, and from Al_2O_3. In the high thickness limit of the film growth process, the ratio approaches that calculated for bulk Al_2O_3, as shown in Figure 9.

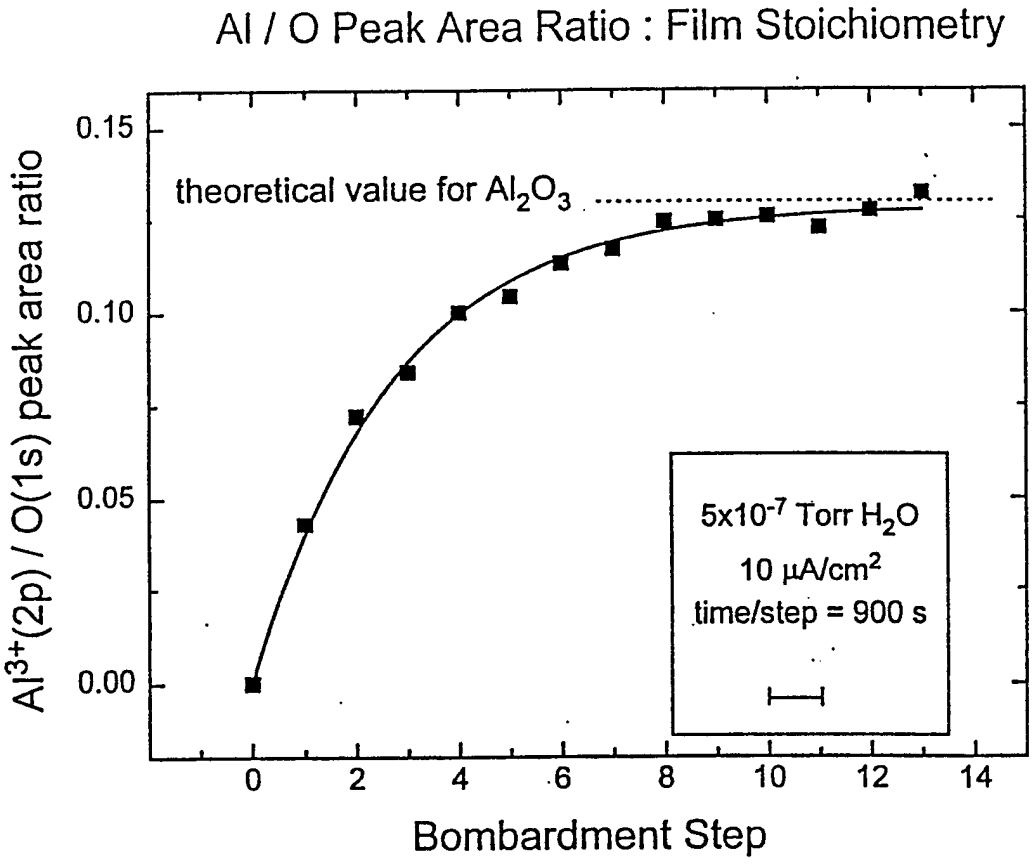

Figure 9. Al^{+3}/O XPS peak area ratio showing the approach to Al_2O_3 stoichiometry as the film thickness approaches 25 Å [6].

The limiting thickness of the deposited Al_2O_3 film was measured by tilting the crystal relative to the detector and measuring the Al^0/Al^{+3} ratio, as shown in Figure 10. The fit of the data to theory shows that a film thickness of 25 Å has been achieved at the shutdown point in the film growth.

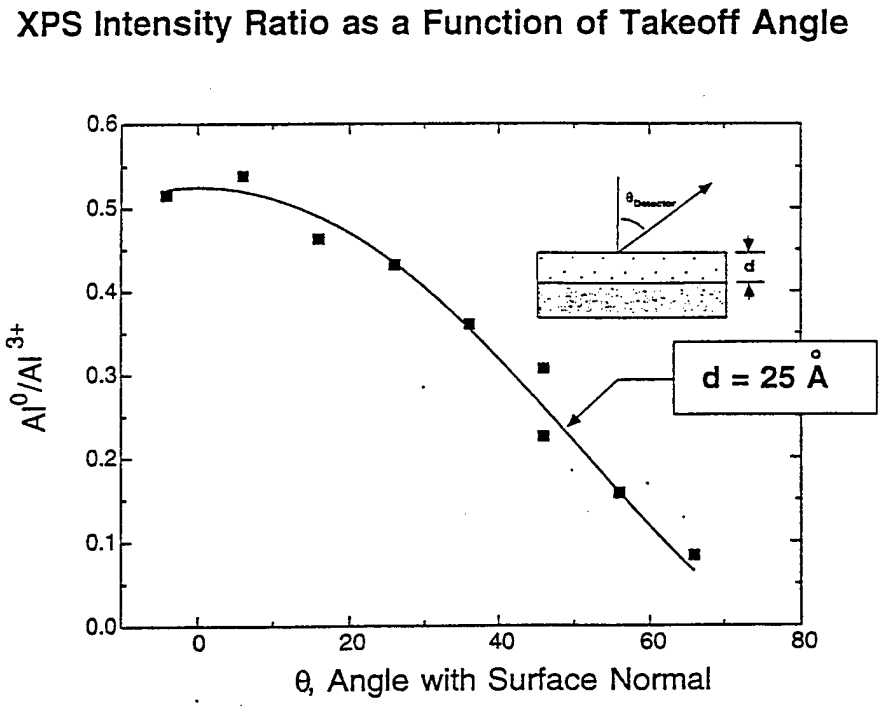

Figure 10. XPS intensity ratio as a function of takeoff angle [6].

The electronic character of the oxide film was measured using electron energy loss spectroscopy (EELS). Incident electrons of 460 eV energy result in the production of scattered electrons with characteristic energy losses which may be used to determine the electronic excitation spectrum of the surface sampled. Thus, in Figure 11, the Al(111) surface, exposed only to 4500 L (1 L = 1 x 10^{-6} Torr s exposure) of H_2O(g) at 300 K, exhibits primarily the loss features of clean aluminum, since only a small coverage of aluminum oxide has been produced by this treatment. Aluminum surface plasmon (10.9 eV) and bulk plasmon (15.7 eV) losses, as well as the combinations of these losses are observed. In contrast, the

surface produced by exposure to H_2O and 100 eV electrons exhibits entirely different loss features, with the prominent loss at 23.5 eV being due to the bulk plasmon of Al_2O_3. The losses characteristic of the clean aluminum surface are not observed because of the relatively large thickness of the Al_2O_3 film produced when electronic excitation is used for growing the film.

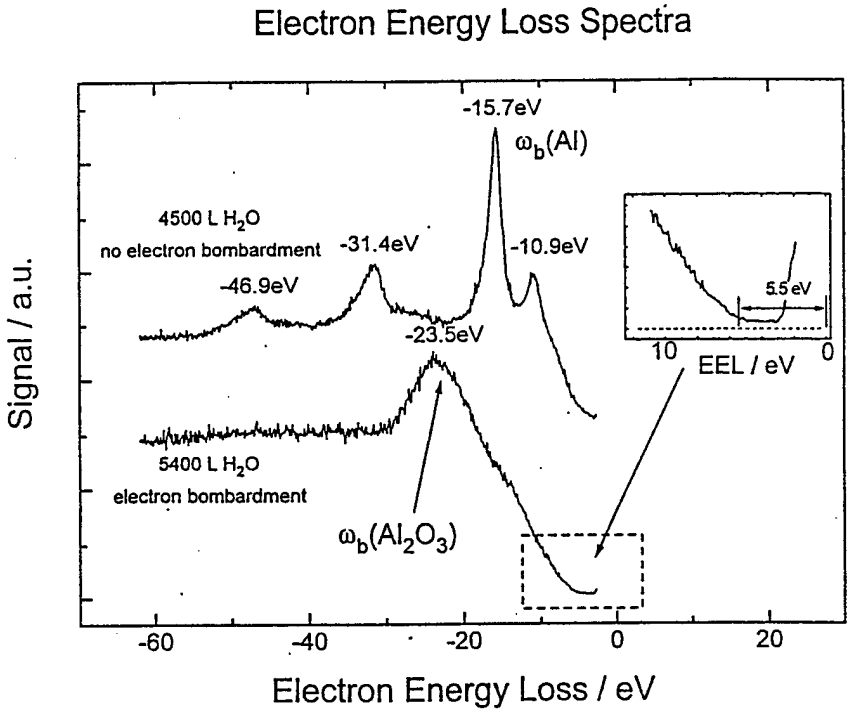

Figure 11. Electron energy loss spectrum for Al(111) exposed to H_2O or to electron-activated H_2O [6].

A second feature in Figure 11, characteristic of the Al_2O_3 film is the 5.5 eV gap between the Fermi level and the onset of the loss spectrum. This indicates a band gap width of about 5.5 eV, which corresponds well to the gap energy measured on sapphire by the same EELS technique[7].

Studies of the scattering of low energy electrons by the Al_2O_3 oxide film indicate that it is very amorphous in character [6]. Nevertheless, the film exhibits the following properties of sapphire:

1. Correct stoichiometry.

2. Correct plasmon loss energy.

3. Correct bandgap.

4. Correct XPS binding energies for Al^{+3} and O^{-2} in Al_2O_3.

D. Kinetics of Al_2O_3 Film Growth Stimulated by Electron Bombardment

The rapid film growth rate under electron bombardment is caused by electron-beam induced dissociation of adsorbed water and enhanced formation of surface oxygen anions. During electron bombardment, according to our measurements [6], the surface excess concentration of negative ions remains constant at a coverage of about 1.4×10^{13} O^{-2}/cm^2 as the film grows. This results in the presence of a **constant electric field** between the metal surface and the outer oxide film surface at all film thicknesses, and this causes a constant flux of ions through the oxide film during its growth, **giving linear growth kinetics**. In contrast to this, a film grown thermally has a decreasing surface charge as the thickness increases, and hence exhibits a decreasing rate of film growth (Mott-Cabrera theory). A schematic diagram of the growing Al_2O_3 film with constant outer surface charge, under the action of electron bombardment, is shown in Figure 12.

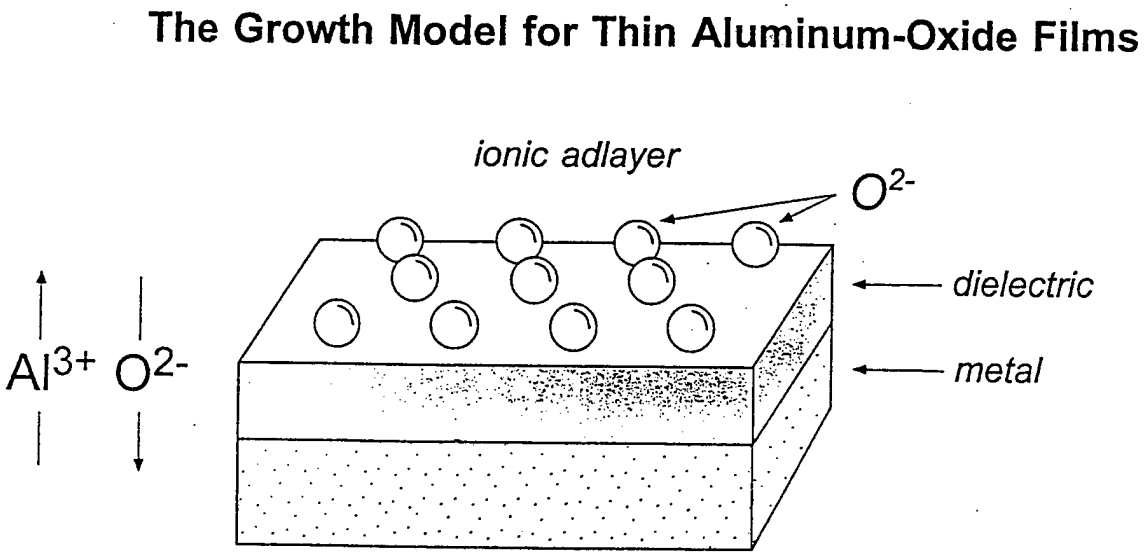

Figure 12. The growth model for thin aluminum oxide films under the influence of water vapor supply and electron bombardment [6].

The presence of a uniform electric field across the growing oxide film was experimentally measured by monitoring the shift of the XPS features of both Al^{+3} and O^{-2} as the film became increasingly thick [6]. Since XPS will detect species within a narrow thickness range, due to electron mean free path considerations, the detected cations and anions present in the surface region of the film will exhibit energy shifts which are influenced by the local electric potential in the sampled region. **Therefore, for a film with a constant electric field across its width, no matter what its width may be, the observed binding energy of the core electrons for both cations and anions should decrease linearly with increasing thickness.** This was experimentally observed as shown in Figure 13. The parallel shift in binding energy for both cations and anions cannot be rationalized chemically, and is due to XPS surface sampling at different positions in the electrostatic potential gradient within the growing oxide film [6]. A constant

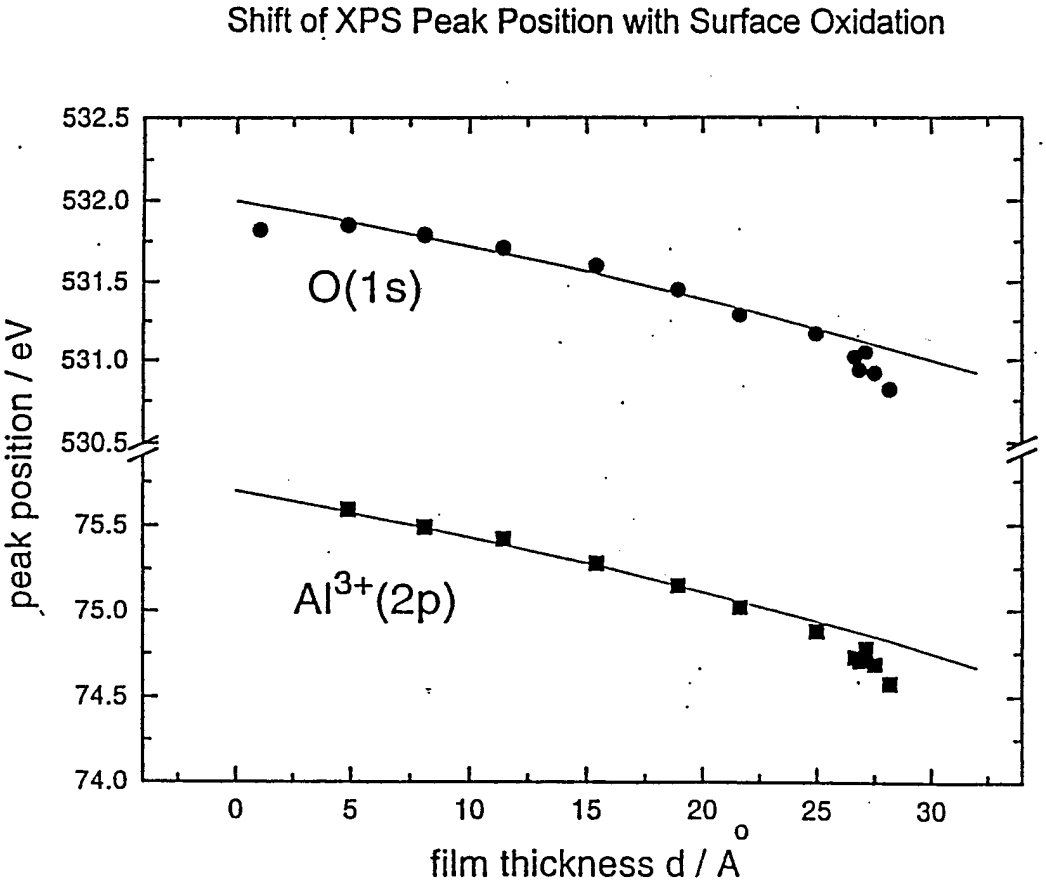

Figure 13. Shift of XPS peak position with increasing oxide film thickness [6].

field strength across the oxide layer of about 5 x 10^6 V/cm, independent of film thickness, was calculated. The breakdown field for Al_2O_3 ranges from 3 - 13 x 10^6 V/cm [9].

The cessation of rapid film growth at a film thickness of about 25 Å (Figure 10) under electron beam stimulation is not understood at the present time [6]. One can imagine the elimination of a favorable ion migration pathway at a critical film thickness. Most likely the ions migrate along defect sites such as those found at Al_2O_3 cluster surfaces, and these favorable transmission pathways might be significantly blocked at a critical film thickness as the clusters of Al_2O_3 coalesce.

E. Electrochemical Testing of Al_2O_3 Films for Corrosion Inhibition

Films of Al_2O_3 on 99.999% pure and atomically clean polycrystalline aluminum surfaces have been grown using exactly the methods employed for the Al(111) surfaces above. A separate UHV system, equipped with all needed facilities was used in these experiments. Both electron impact oxidation (100 eV excitation at 10μA/cm^2 using incident water vapor at 5 x 10^{-7} Torr) and air oxidation (at one atmosphere) of atomically clean aluminum have been carried out in a large number of experiments to compare the electrochemical corrosion inhibition properties of each type of oxide film [9].

The films prepared by electronic excitation are remarkable when compared to those prepared by ordinary air oxidation as indicated in the electrochemical impedance spectra (EIS) of Figure 14. A large number of experiments are compared in Figure 16 to be sure that the statistical spread of the results do not confound the comparison. The electrical impedance, measured at the plateau near zero frequency (DC) conditions, of the electron-impact produced films is about 30 times higher than that found for the air-oxidized films! **This suggests that enhanced corrosion inhibition is very likely for the high impedance aluminum oxide films produced by electron bombardment of adsorbed water on aluminum surfaces.**

THE COMPARISON IS EVEN MORE REMARKABLE WHEN ONE REALIZES THAT THE EXPOSURE TO OXYGEN (AS WATER) IN THE ELECTRON IMPACT EXPERIMENTS IS ONLY 10^{-10} OF THE OXYGEN EXPOSURE IN THE AIR!!!!

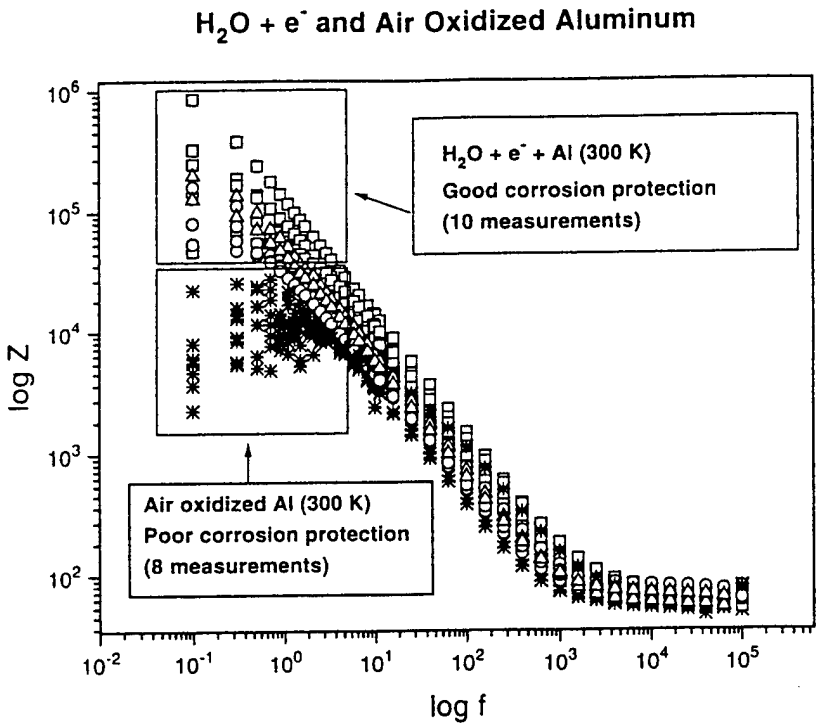

Figure 14. Electrochemical impedance spectroscopy of aluminum oxide films produced by electron bombardment of adsorbed water and by air oxidation [9]. Z is the impedance of the film plus electrolyte, plotted vs. AC frequency, f.

III. Status of Effort - Behavior of Corrosion Inhibitor Molecules on Al_2O_3 Surfaces

A. Benzotriazole (BTAH)- Bonding to Al_2O_3 Surfaces as Revealed by Infrared Spectroscopy

This molecule is a well known corrosion inhibitor on copper surfaces, and it is postulated that a nitrogen atom within the triazole ring bonds to Cu^+ sites in Cu_2O films on Cu surfaces. The close packing of the aromatic rings within the layer then forms a physical barrier to the penetration of corrosive species into the metal surface. A schematic diagram of the bonding of this heterocyclic molecule to a surface containing a Cu_2O film is shown in Figure 15, where the off-axis N atom in the triazole ring, possessing more electric charge than the N atom on the

C_2 axis, is the donor atom linking the molecule to the Cu^+ cation site [10].

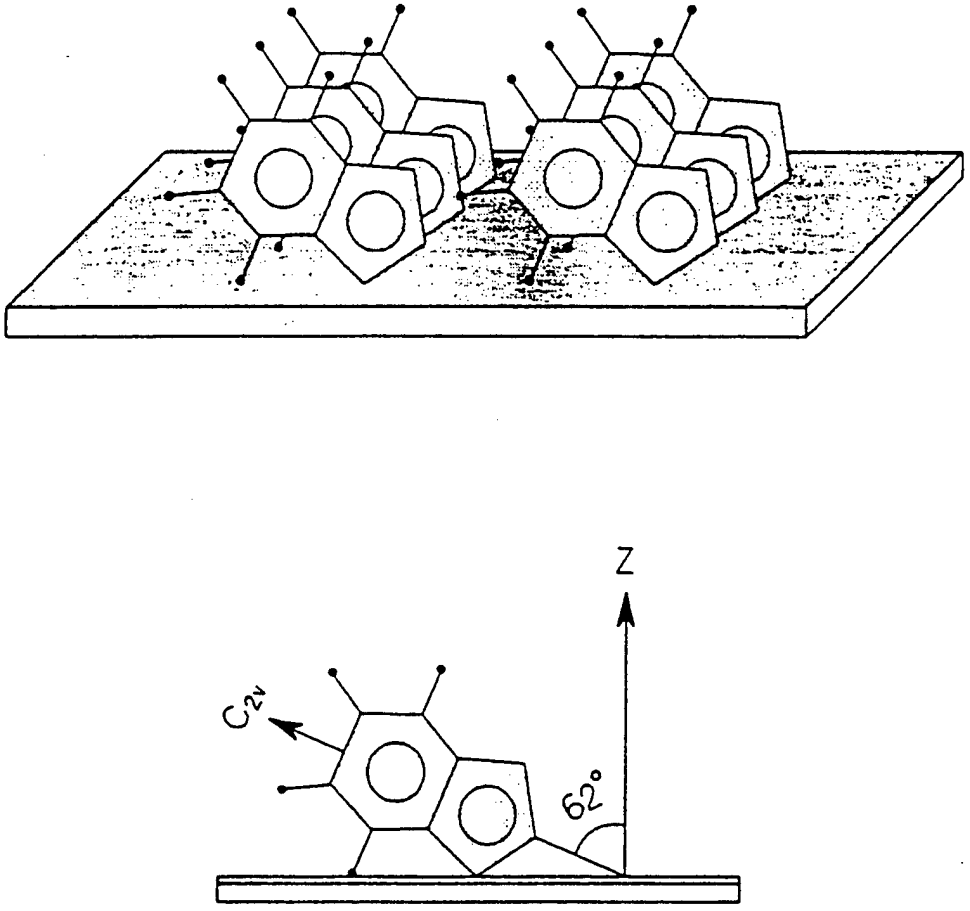

Figure 15. Proposed structure of BTA^- on a Cu_2O/Cu surface [10].

We postulated in our previous AFOSR proposal that the BTAH molecule, following deprotonation to produce the anion BTA^-, would similarly bond to Lewis acid (Al^{+3}) sites on Al_2O_3 surfaces. Transmission FTIR studies of BTAH adsorption onto powdered Al_2O_3 surfaces were performed [11], and very interesting results were obtained. The special FTIR cell used for this work (see Figure 16) contains an internal support for the Al_2O_3 powder on a fine tungsten grid. The grid and the supported Al_2O_3 temperature may be accurately controlled in the range 150 K to 1500 K. A specially designed doser, which is temperature controlled by good heat conduction along its length, is aimed at the Al_2O_3 surface and provides well controlled doses of the adsorbate. Solid BTAH has a low vapor pressure at room temperature [11].

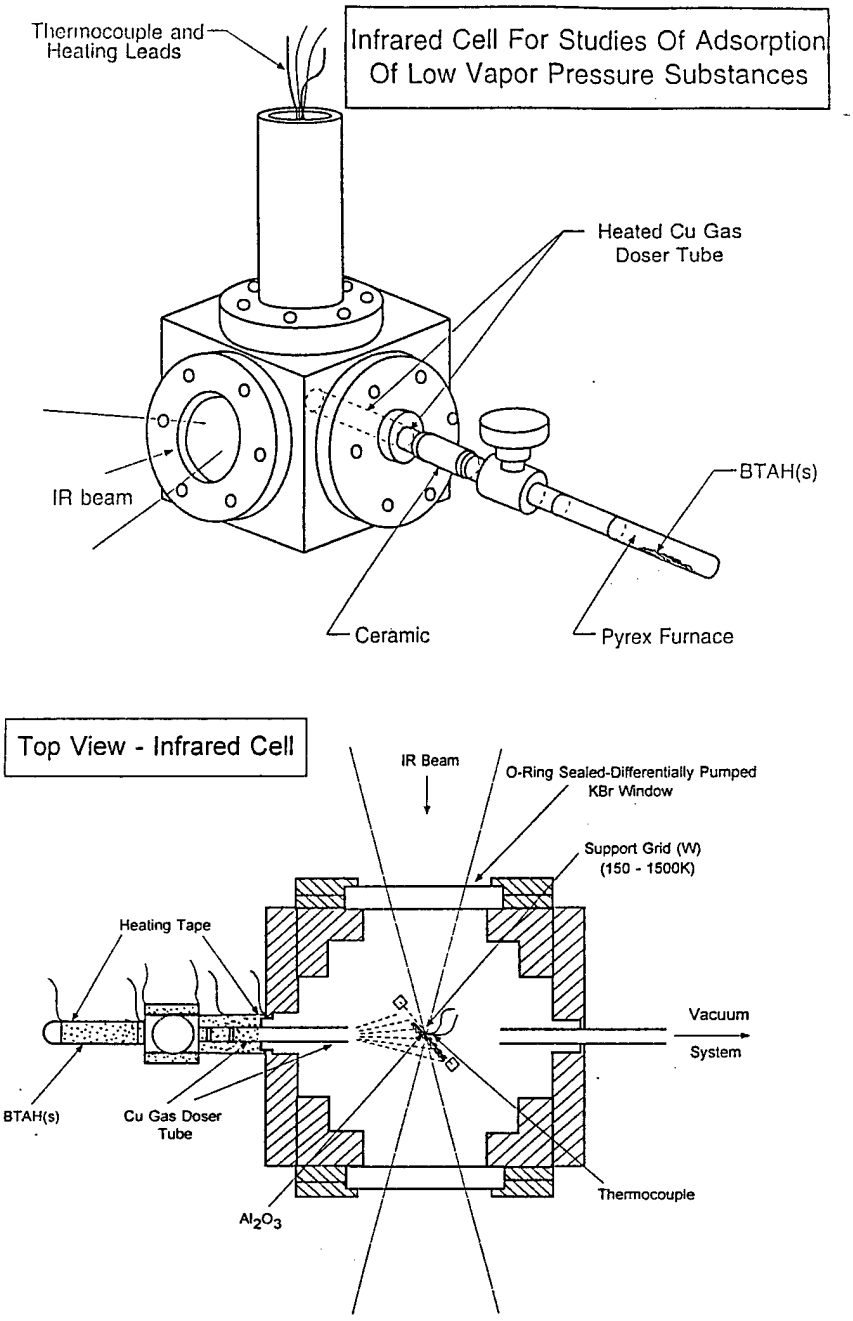

Figure 16. Transmission FTIR cell for the deposition and spectroscopic study of a low vapor pressure compound on a high area surface [11].

A typical spectrum, showing the preferential bonding of the BTAH molecule with isolated hydroxyl groups on the surface at 293 K is shown in Figure 17. The isolated hydroxyl groups are quantitatively converted to associated hydroxyl groups by this interaction as the BTAH exposure is increased (note the isobestic point). This occurs by hydrogen bonding of surface Al-OH groups to the triazole ring system without appreciable deprotonation of the BTAH molecule, and represents the first step in surface bonding of BTAH to the hydroxylated Al_2O_3 surface [11].

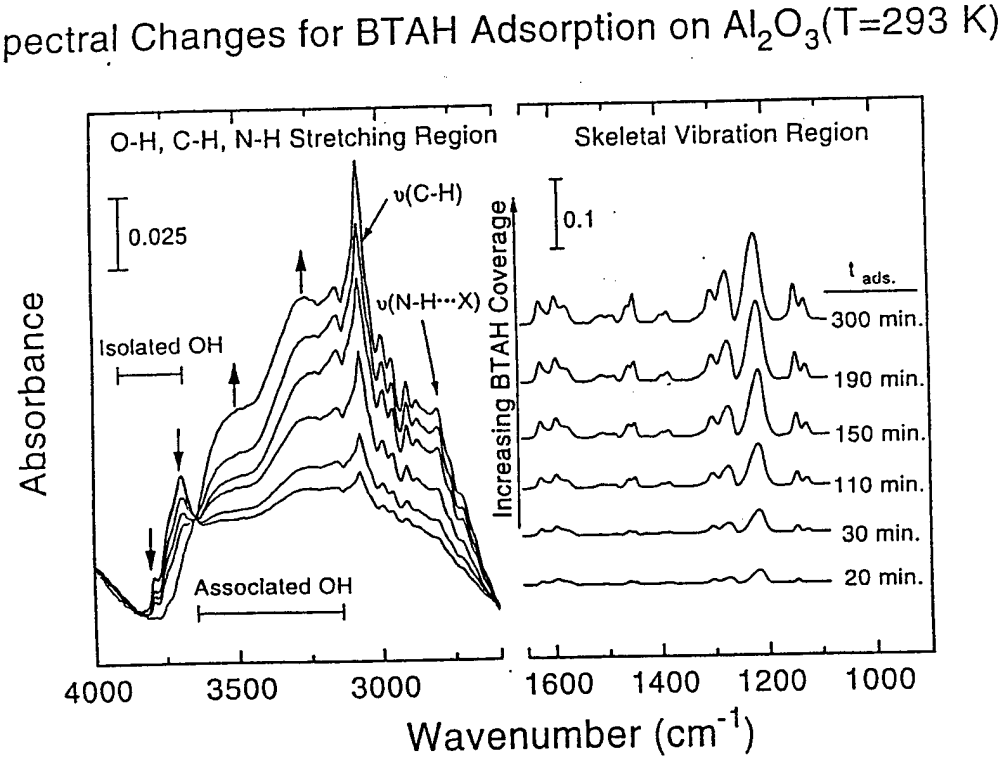

Figure 17. Spectral changes for BTAH adsorption on Al_2O_3 (T=293 K) [11].

The deprotonation of the BTAH molecule to produce BTA^- anions occurs over the temperature range ~ 273 K to 453 K. This is accompanied by the massive production of new Al-OH groups from interaction of the proton of BTAH with Lewis base (Al-O-Al) sites, as shown in Figure 18.

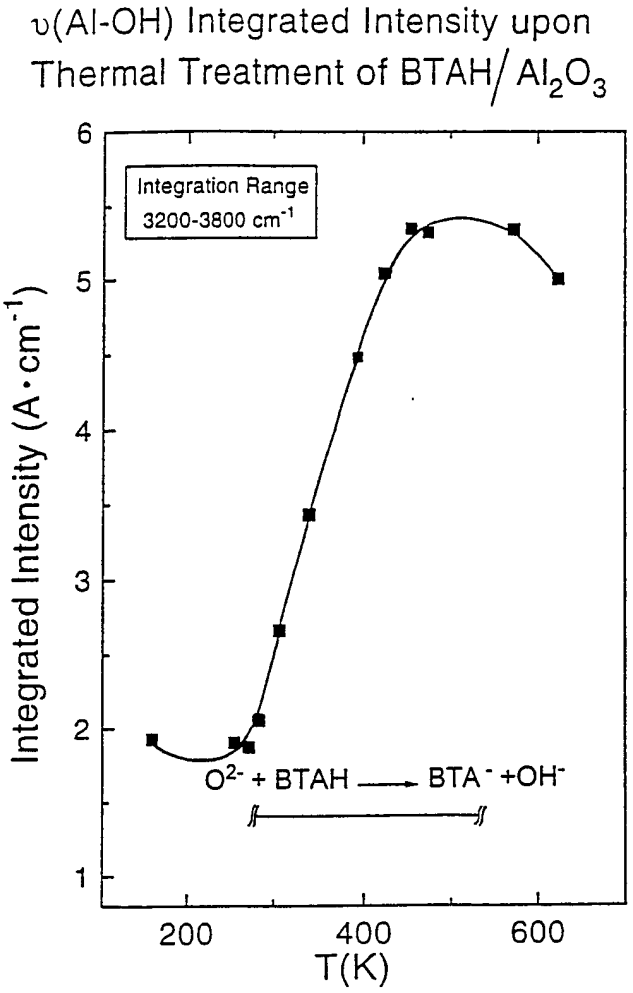

Figure 18. Production of surface hydroxyl groups from the deprotonation of BTAH on Al_2O_3 [11].

As the deprotonation of BTAH occurs over the temperature range 273 K to 453 K, infrared modes characteristic of the anion, BTA^-, also develop, as shown in Figure 19.

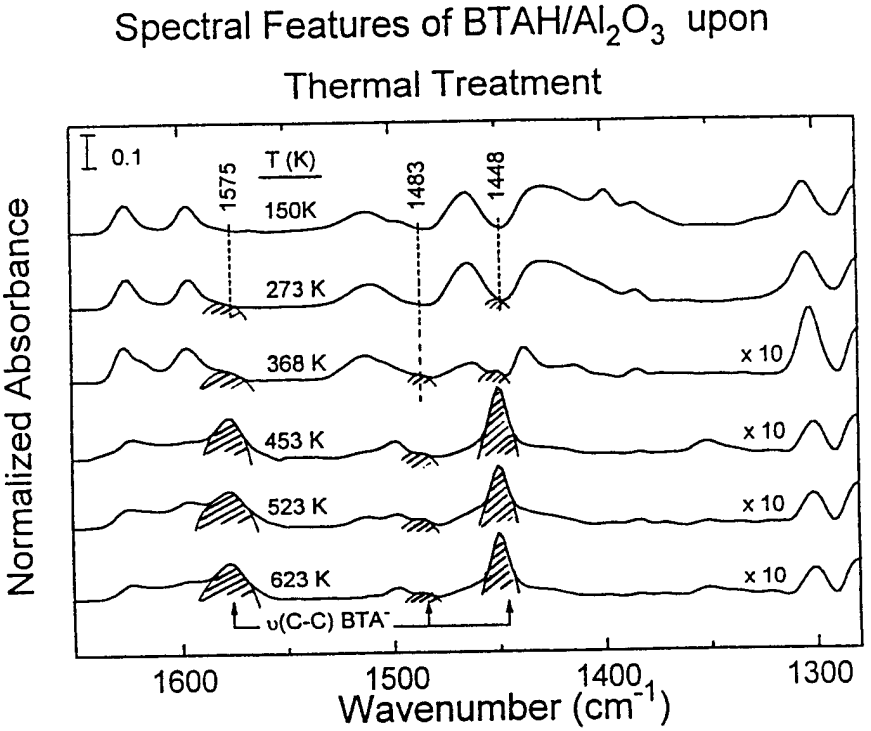

Figure 19. The production of BTA- anions on Al_2O_3 surfaces [11].

A summary of the various bonding modes and the high temperature decomposition of the BTAH molecule adsorbed on Al_2O_3 is shown in Figure 20. The information gained about the temperature ranges associated with various BTAH surface reaction processes will be very helpful in future studies of the corrosion inhibition behavior of this molecule on aluminum surfaces. For example, the results show that BTAH treatment near room temperature will mainly produce BTAH molecules bonded to surface hydroxyl groups. Heating to about 453 K will produce a maximum surface coverage of more strongly bound BTA- anions linked by nitrogen donor atoms to Lewis acid Al^{+3} sites. **Thus the production of an effective corrosion inhibitor layer on Al_2O_3/Al will require thermal activation above room temperature.** The infrared spectroscopy results further show that the BTA- anion on Al_2O_3 is stable to about 573 K, before

decomposing by the fragmentation of the triazole ring.

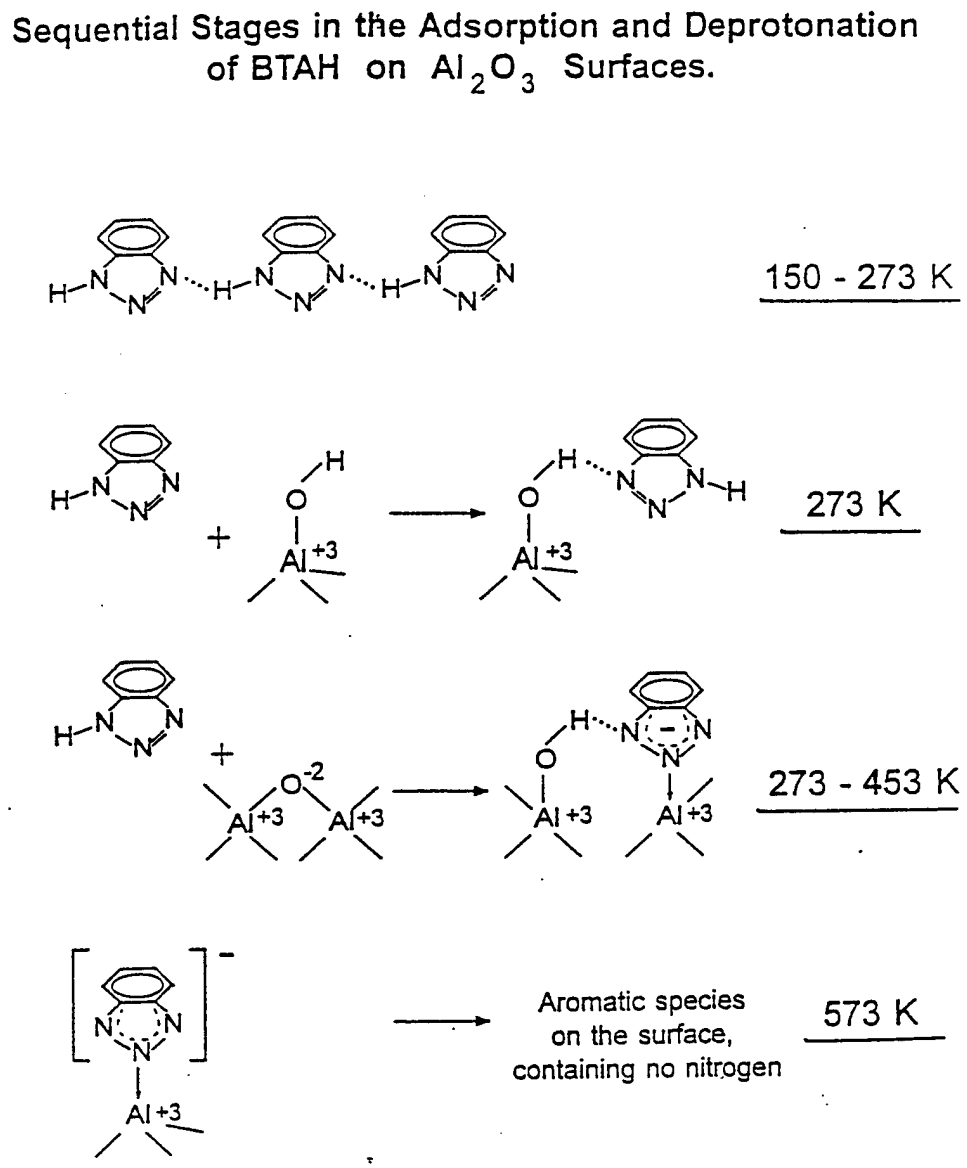

Figure 20. Sequential stages in the adsorption and deprotonation of BTAH on Al_2O_3 surfaces [11].

B. Silanol Corrosion Inhibition on Al_2O_3 Surfaces

A recent Russian paper indicated that dramatic corrosion inhibition effects were observed for particular silanol-derived overlayers adsorbed on Al_2O_3 layers on Al surfaces [12]. The molecule, vinyltriethoxysilane, CH_2=$CHSi(OC_2H_5)_3$, (VTES) resulted in a layer of about 100 Å thickness. This film caused an increase of 250 mV in the Al pitting potential [12]. Localized corrosion was strongly inhibited [13].

We therefore decided to investigate the adsorption and decomposition of VTES on powdered Al_2O_3 surfaces, as was done for the BTAH molecule in Section III A, above.

Figure 21 shows a schematic reaction scheme for the VTES molecule with the Al_2O_3 surface [14], as deduced from observations of the infrared spectrum of the adsorbed layer as a function of temperature. Upon adsorption and in the first stage of reaction, (Figure 21 A), VTES seeks isolated Al-OH groups, and bonds through interaction of the the ethoxy functionality, eliminating ethanol and forming linkages with the surface to the silicon atom of the silanol. The second observed stage of interaction (Figure 21 B) involves continued reaction with Al-OH groups, making more surface linkages of the silicon atom of the silanol to the surface, and evolving more ethanol. This second stage reaction begins at 520 K. The third stage of reaction involves loss of the vinyl groups, with the evolution of ethylene gas, and begins at 820 K. Thus, the ethoxy groups are the most reactive groups on the molecule, and the vinyl groups are more stable. After the loss of the vinyl groups, a silicate-type overlayer remains on the surface, and exhibits a strong isolated SiO-H stretching mode.

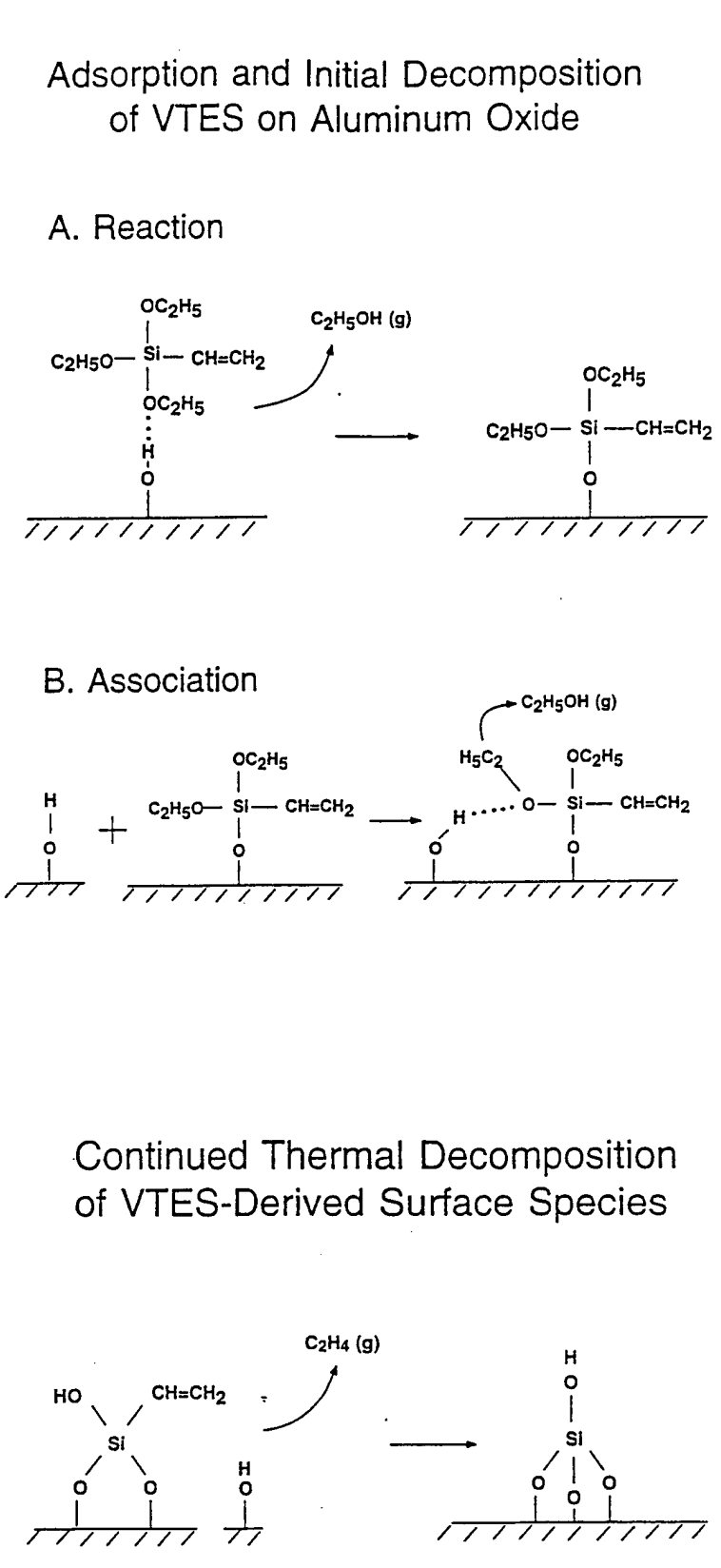

Figure 21. Sequence of adsorption, dissociation, and final decomposition processes for the VTES molecule on Al_2O_3 [14].

The ability of infrared spectroscopy to map out the various stages of thermal decomposition is illustrated in Figure 22, where the dependence of the intensity of an ethoxy mode and the vinyl mode are plotted together versus temperature. One may clearly see the onset of the ethoxy decomposition at 520 K, and the higher temperature of onset of vinyl decomposition at 820 K. The Figure also shows the infrared spectrum of the gas phase observed above the heated layer. In the final stages of heating, all ethanol in the gas phase has been decomposed to ethylene gas.

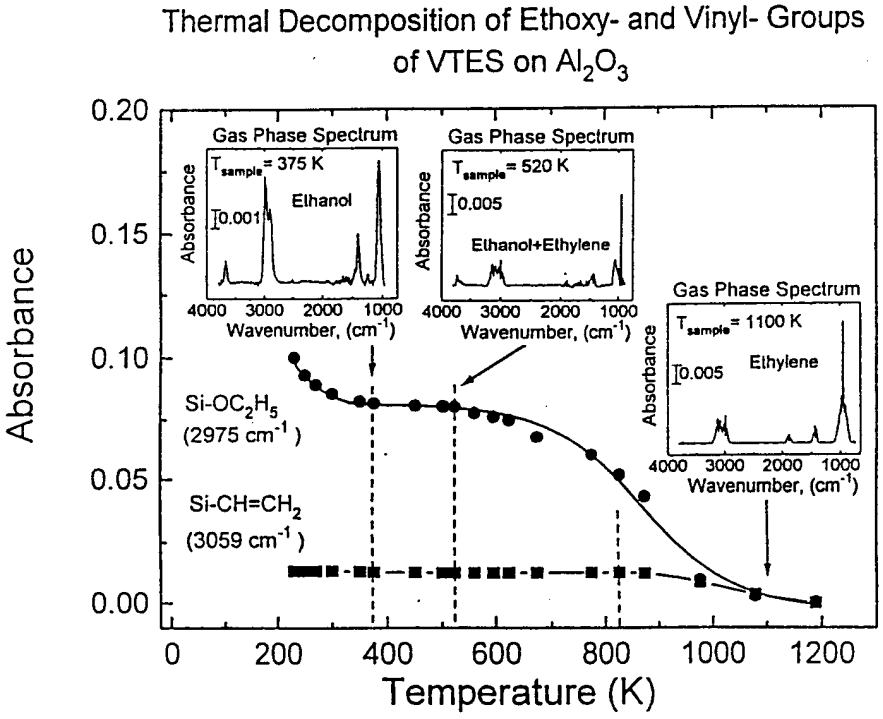

Figure 22. Thermal decomposition of ethoxy- and vinyl- groups of VTES on Al_2O_3 [14].

IV. Summary of Published and submitted Papers, April 1, 1995 - June 30, 1997.

A total of 14 papers and reviews have been submitted or published in the 27 months of this AFOSR grant. Of these, three review articles were produced including a definitive review of the surface chemistry of diamond (item 481) which occupied 3 consecutive issues of the review journal and contained a cross referenced bibliography of over 900 articles. In addition, an article describing a novel method for the fluorination of diamond surfaces was published in Science

(item 462). Finally, a cooperatively written article with Professor W. A. Goddard III and his postdoctoral student, Dr. X. Chen, of Caltech (item 485) provided the details of the research findings for diamond fluorination along with theoretical calculations of XPS chemical shifts and molecular dynamic behavior of adsorbed perfluoroalkyl groups on diamond(100) surfaces. The list of articles is given below:

432. A. Szabó and J. T. Yates, Jr., "Isotope Effect in Electron Stimulated Desorption - The Role of Internal Degrees of Freedom in CO Desorption from Pt(111)," J. Chem. Phys. 102, 563 (1995).

451. J. T. Yates, Jr., "Surface Chemistry at Metallic Step Defect Sites," J. Vac. Sci. Technol. A 13, 1359 (1995).

452. V. S. Smentkowski, H. Jänsch, M. A. Henderson and J. T. Yates, Jr., "Deuterium Atom Interaction with Diamond(100) Studied by X-Ray Photoelectron Spectroscopy," Surface Science 330, 207 (1995).

462. V. S. Smentkowski and J.T. Yates, Jr., "Fluorination of Diamond Surfaces - A Facile New Method," Science 271, 193, (1996).

465. J. T. Yates, Jr., "Electron Stimulated Desorption-Ion Angular Distribution (ESDIAD): A Method for Imaging Chemical Bond Directions and Thermal Disorder in Adsorbed Species," Handbook of Surface Imaging and Visualization, CRC Press, Inc., Chapter 12, p. 157 (1995).

466. V.S. Smentkowski and J.T. Yates, Jr., "Universal Calibration of W5%Re vs. W26%Re (Type-C) Thermocouples in the Temperature Range 32 K to 2588 K," J. Vac. Sci. Techno. A 14, 260 (1996)

468. V. S. Smentkowski and J.T. Yates, Jr., "Fluoroalkyl Iodide Photodecomposition on Diamond (100) - An Efficient Route to the Fluorination of Diamond Surfaces," Mat. Res. Soc. Symp. Proc. 416, 293 (1996).

481. J. Wei and J. T. Yates, Jr., "Diamond Surface Chemistry I - A Review," and J. Wei, V. S. Smentkowski and J. T. Yates, Jr., "Diamond Surface Chemistry II - Selected Bibliography," Critical Reviews in Surface Chemistry, Volume 5/Issues 1-3 (1995).

485. V. S. Smentkowski, X. Chen, W. A. Goddard III and J. T. Yates, Jr., "Fluorination of Diamond - C_4F_9I and CF_3I Photochemistry on Diamond (100)," Surface Science 370, 209 (1997).

497. T. W. Barefoot, H. D. Ebinger and J. T. Yates, Jr., "Low Energy Broad Beam Electron Gun," J. Vac. Sci. Technol. A15, 2740 (1997).

501. H. D. Ebinger and J. T. Yates, Jr., "Oxidation of Al(111) by Electron Impact on Adsorbed H_2O" in press, Surface Science.

503. A. Kuznetsova, E. A. Wovchko and J. T. Yates, Jr., "FTIR Study of the Adsorption and Thermal Behavior of Vinyltriethoxysilane Chemisorbed on γ-Al_2O_3," Langmuir 13, 5322 (1997).

508. H. D. Ebinger and J. T. Yates, Jr., "Electron Impact Induced Oxidation of Al(111) in Water Vapor - Relation to the Cabrera-Mott Mechanism," Phys. Rev. B 57, 1976 (1998).

512. I. Popova and J. T. Yates, Jr., "Adsorption and Thermal Behavior of Benzotriazole Chemisorbed on γ-Al_2O_3," Langmuir 13, 6169 (1998).

V. Personnel

The following staff members are currently working on the AFOSR funded project:

1. Ms. Anya Kuznetsova, 2nd year graduate student.
2. Ms. Irene Popova, 1st year graduate student.
3. Mr. Vasily Fomenko, 1st year graduate student.
4. Dr. Vladimir Zhukov, postdoctoral fellow.

References

[1] H. Ebinger and J.T. Yates, Jr., Surface Science, in press.

[2] C.E. Melton, J. Chem. Phys. 57, 4218 (1972).

[3] M. Jungen, J. Vogt, and V. Staemmler, Chem. Phys. 37, 49 (1979).

[4] M.G. Curtis and I.C. Walker, J. Chem. Soc. Far. 88, 2805 (1992).

[5] D. Klyachko, P. Rowntree and L. Sanche Surf. Sci. 346, L49 (1996).

[6] H.D. Ebinger and J.T. Yates, Jr. Phys. Rev. B 57,1976 (1998).

[7] M.A. Schildbach and A.V. Hansma, Surf. Sci., 282, 306 (1993).

[8] N. Klein and M. Albert, J. Appl. Phys. 53, 5840 (1982).

[9] A. Kuznetsova, T.D. Burleigh, V. Zhukov, J. Blachere and J.T. Yates, Jr., Langmuir 14, 2502 (1998).

[10] Z. Xu, S. Lau, and P.W. Bohn, Surf. Sci. 296, 57 (1993).

[11] I. Popova and J.T. Yates, Jr., Langmuir 13, 6169 (1997).

[12] A.P. Nazarov, M.A. Petrunin, and Yu.N. Mikhailovskii, Translated from: Zashchita Metallov 28, 564-574, July-August 1992. Original article submitted January 30, 1991.

[13] A.P. Nazarov, M.A. Petrinin, Yu.N. Mikhailovskii, Zashchita Metallov 26, 970 (1990).

[14] A. Kuznetsova, E. Wovchko, and J.T. Yates, Jr., Langmuir 13, 5322 (1997).